Available online at www.sciencedirect.com
ScienceDirect
International Journal of Heat and Fluid Flow 28 (2007) 429–440
International Journal of HEAT AND FLUID FLOW
www.elsevier.com/locate/ijhff

Application of linear and non-linear low-*Re* k–ε models in two-dimensional predictions of convective heat transfer in passages with sudden contractions

M. Raisee *, S.H. Hejazi

Department of Mechanical Engineering, University of Tehran, P.O. Box 11365/4563, Tehran, Iran

Received 9 August 2004; received in revised form 15 June 2006; accepted 13 July 2006
Available online 7 September 2006

Abstract

This paper presents comparisons between heat transfer predictions and measurements for developing turbulent flow through straight rectangular channels with sudden contractions at the mid-channel section. The present numerical results were obtained using a two-dimensional finite-volume code which solves the governing equations in a vertical plane located at the lateral mid-point of the channel. The pressure field is obtained with the well-known SIMPLE algorithm. The hybrid scheme was employed for the discretization of convection in all transport equations. For modeling of the turbulence, a zonal low-Reynolds number k–ε model and the linear and non-linear low-Reynolds number k–ε models with the "Yap" and "NYP" length-scale correction terms have been employed. The main objective of present study is to examine the ability of the above turbulence models in the prediction of convective heat transfer in channels with sudden contraction at a mid-channel section. The results of this study show that a sudden contraction creates a relatively small recirculation bubble immediately downstream of the channel contraction. This separation bubble influences the distribution of local heat transfer coefficient and increases the heat transfer levels by a factor of three. Computational results indicate that all the turbulence models employed produce similar flow fields. The zonal k–ε model produces the wrong Nusselt number distribution by underpredicting heat transfer levels in the recirculation bubble and overpredicting them in the developing region. The linear low-*Re* k–ε model, on the other hand, returns the correct Nusselt number distribution in the recirculation region, although it somewhat overpredicts heat transfer levels in the developing region downstream of the separation bubble. The replacement of the "Yap" term with the "NYP" term in the linear low-*Re* k–ε model results in a more accurate local Nusselt number distribution. Moreover, the application of the non-linear k–ε model further improves the thermal predictions. In general, among the three turbulence models examined, the non-linear low-*Re* k–ε model produces the best heat transfer predictions.

Keywords: Sudden contraction; Turbulent heat transfer; Turbulence modeling

1. Introduction

Cooling passages of modern gas turbine blades contain several complex geometrical features such as ribs, 180° bends, and sudden contractions at the inlet (see Fig. 1). These features strongly influence the behavior of the flow and heat transfer and consequently affect the cooling performance. Detailed information about flow and heat transfer in internal cooling channels of advanced gas turbine blades can be very valuable for the design of the new generation of the gas turbines in which the turbine inlet temperature exceeds 2000 K. To obtain such information experimentally can be very difficult and expensive. The only other method for producing the details of the flow and thermal fields is to solve the governing equations of the flow and energy. However, flows in internal cooling channels are turbulent and their prediction requires the use of turbulence models. Such models need to be able to

* Corresponding author.
E-mail address: mraisee@ut.ac.ir (M. Raisee).

0142-727X/$ - see front matter © 2006 Elsevier Inc. All rights reserved.
doi:10.1016/j.ijheatfluidflow.2006.07.004

Nomenclature

A	cross-section area
c_p	specific heat transfer capacity at constant pressure
D	height of channel after contraction
$D_h = 4A/P$	hydraulic diameter of channel after contraction
h	contraction height
H	channel height before contraction
k	turbulent kinetic energy
$\dot{m}$	mass flow rate
Nu	local Nusselt number
$Nu_{fd} = 0.023Re^{0.8}Pr^{0.4}$	fully developed Nusselt number
P	cross-sectional perimeter
Pr	Prandtl number
q''_w	local wall heat flux
S_θ	extra source term in the discretized energy equation
$Re = U_{in}D_h/\nu$	Reynolds number
U_i	mean velocity components (U, V)
U_{in}	uniform inlet velocity
$\overline{u_i u_j}$	Reynolds stress tensor
$\overline{u_i\theta}$	turbulent heat flux tensor
W	channel width
x_i	Cartesian coordinates (x, y)
x	axial distance from the contraction
y	normal distance to the wall
$y^* = \frac{\nu\sqrt{k}}{\nu}$	turbulent Reynolds number

Greek symbols

δ_{ij}	Kronecker delta
ε	dissipation rate
Θ_b	cross-section-averaged temperature
Θ_w	wall temperature
κ	thermal conductivity
μ	dynamic viscosity
ν	kinematic viscosity
ρ	density

cope, among other things, with the presence of curvature-induced secondary motions, the presence of separation caused by a sudden change in cross-section and also be sensitive to the effects of Coriolis forces on the turbulence. In the present contribution, attention is focused solely on effects of channel contraction.

There already are a number of publications in literature that experimentally studied the effects of a sudden contraction on characteristics of flow and heat transfer. Sparrow and Cur (1982), using naphthalene method, reported local heat transfer measurements for turbulent air flow in a symmetrical and asymmetrical heated straight rectangular duct with a sudden contraction at inlet. Heat transfer experiments were performed for a high-aspect-ratio rectangular duct having a sharp-edge inlet. The Reynolds number was varied from 10^4 to 4.5×10^4. They showed that the highest heat transfer coefficient occurs at a location close to the point of flow reattachment. Moreover, they found that at the lower Reynolds number the maximum Nusselt number is about four times the fully developed value, whilst at the higher Reynolds number this reduces to three. Han and Park (1988) studied developing turbulent heat transfer in a rectangular channel with a sudden contraction at inlet and ribs along two opposite walls. The Reynolds number was varied from 5×10^3 to 5×10^4. The contraction ratios were 3 and 6 and the duct aspect-ratio was 4, all these geometrical dimensions being consistent with those found in the cooling passages of gas turbine blades. They showed that flow separation and reattachment at, and downstream of, the channel contraction resulted in high

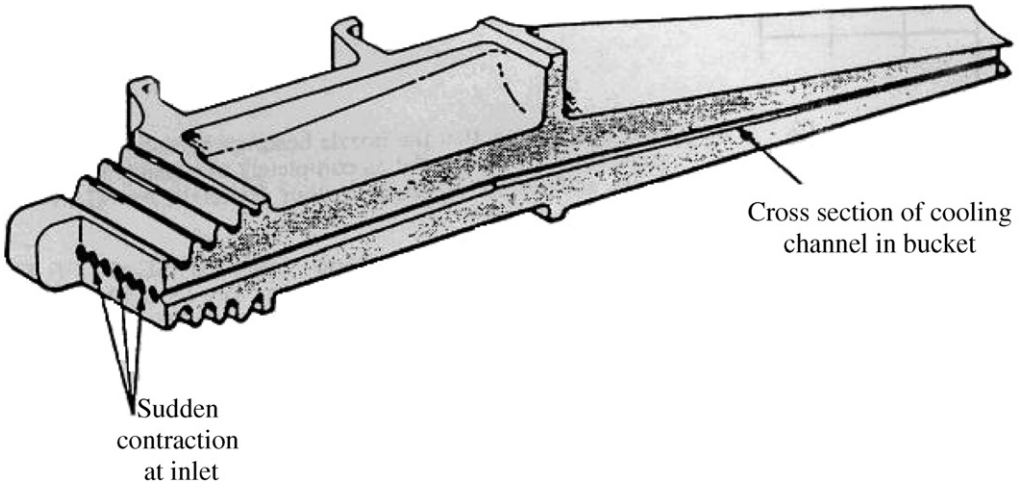

Fig. 1. Schematic of cooling channel with sudden contraction at the inlet.

heat transfer levels. Liou and Hwang (1992) investigated local heat transfer characteristics of developing turbulent flow in a rectangular duct with an abrupt contraction entrance at a Reynolds number of 1.26×10^4. They showed that flow separation at the duct inlet plays an important role in the axial distribution of the heat transfer coefficient in the thermal entrance region. Moreover, the results of their study were in good agreement with those reported by Han and Park (1988).

To the knowledge of the authors, the effects of sudden contraction at the channel inlet have not been numerically examined to date and the present contribution is the first such study. The main objectives of the present investigation are to understand how the sudden contraction alters flow and heat transfer development and to examine the effectiveness of the zonal k–ε model, the linear low-Re k–ε model, and a recently modified non-linear k–ε model in predicting thermal characteristics in such geometries. It is worth mentioning that the cubic non-linear k–ε model has been recently applied for the computations of convective heat transfer in impinging and separating flows by Craft et al. (1999), in ribbed cooling passages by Raisee et al. (2003) and prediction of flow characteristic in curved passages by Raisee et al. (2006) with encouraging success. Thus, the present study further examines the capabilities of the non-linear k–ε model in prediction of convective heat transfer in passages with sudden contractions.

2. Cases examined

Fig. 2 shows the geometry of the channel with a sudden contraction at the mid-channel section. Channel lengths upstream and downstream of the channel contraction are 20 h and 24 h, respectively. The contraction ratio, H/D, is 3.75. For this geometry the reported experimental data consist of local Nusselt number distributions measured for air ($Pr = 0.71$) by Sparrow and Cur (1982) at a Reynolds number of 4.5×10^4 and by Han and Park (1988) at a Reynolds number of 3.0×10^4. The local Nusselt number is defined as

$$Nu = \frac{q''_w D_h}{\kappa(\Theta_w - \Theta_b)}, \tag{1}$$

where q''_w is the local heat flux, κ the fluid conductivity, D_h the hydraulic diameter, Θ_w the wall temperature and Θ_b the bulk temperature.

For both sets of experiments Reynolds number is based on the hydraulic diameter and the bulk velocity after the channel contraction. The channel aspect-ratio, W/D, is 18 at the Reynolds number of 4.5×10^4 and 4 at the Reynolds number of 3.0×10^4. In this study the effects of side walls were ignored and computations were performed only in a vertical plane located at the lateral mid-point of the channel. Although the three-dimensional effects are more pronounced in the second geometry ($W/H = 4$) than that in the first one ($W/D = 18$), however, recent computations of turbulent flow through rectangular ducts of similar aspect-ratio by Raisee et al. (2006), for which the secondary velocity vectors and stream-wise velocity contours at a section in the developing region are shown in Fig. 3, indicates that the side wall effects are insignificant and flow field can be treated as two-dimensional.

For heat transfer computations, a constant heat flux boundary condition is applied on the walls of channel downstream of the contraction and all other walls are assumed to be adiabatic.

3. Flow equations

All the flow equations are presented in Cartesian tensor notation.

3.1. Mean flow equations

For a steady incompressible flow, the conservation laws of mass, momentum and energy may be written as

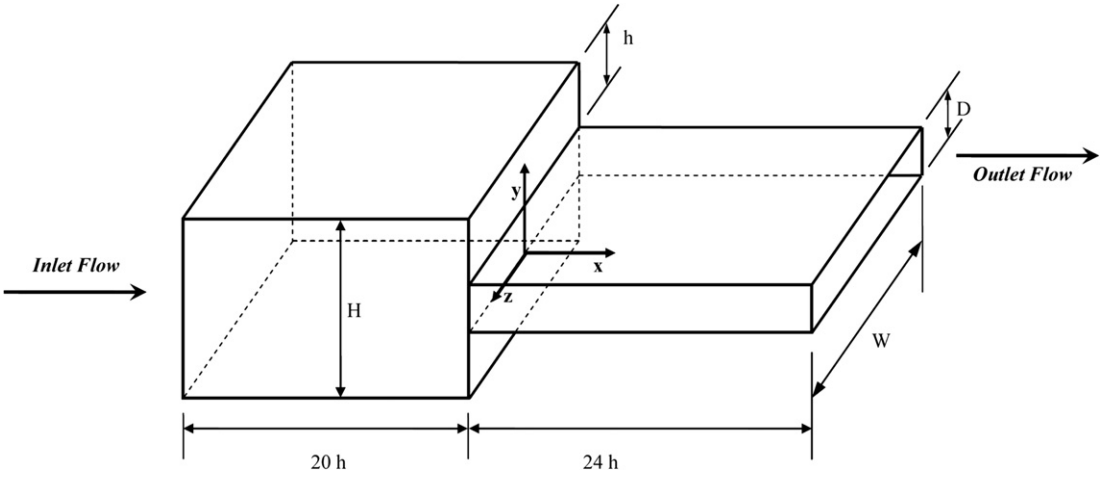

Fig. 2. Flow geometry of rectangular channel with sudden contraction examined.

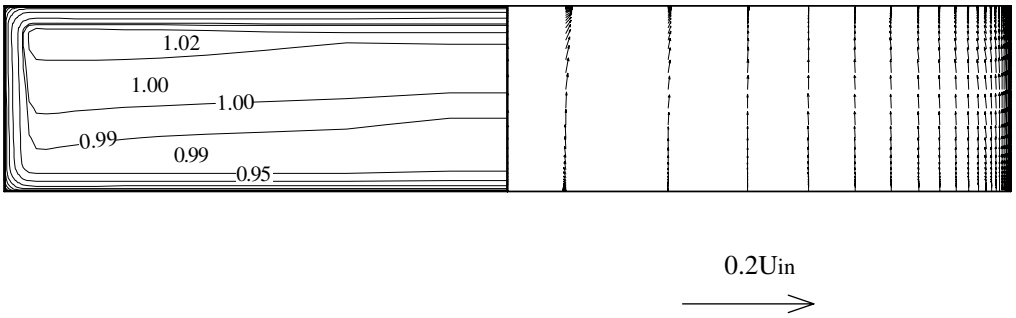

Fig. 3. Predicted stream-wise velocity, U/U_{in}, contours (left), and secondary flow vectors (right) for developing turbulent flow through a rectangular cross-section channel, using the non-linear k–ε model (from Raisee et al., 2006).

Continuity

$$\frac{\partial U_j}{\partial x_j} = 0 \tag{2}$$

Momentum

$$\frac{\partial (U_j U_i)}{\partial x_j} = -\frac{1}{\rho}\frac{\partial P}{\partial x_i} + \frac{\partial}{\partial x_j}\left(\nu \frac{\partial U_i}{\partial x_j} - \overline{u_i u_j}\right) \tag{3}$$

Energy

$$\frac{\partial (U_j \Theta)}{\partial x_j} = \frac{\partial}{\partial x_j}\left(\frac{\nu}{Pr}\frac{\partial \Theta}{\partial x_j} - \overline{u_j \theta}\right) \tag{4}$$

3.2. Turbulence model equations

The turbulence models employed for computation are a zonal k–ε model (Bo et al., 1991), the low-*Re* Launder and Sharma (1974) k–ε model, and a modified version of non-linear low-*Re* k–ε model (Craft et al., 1999). Computations with both the linear and the non-linear low-*Re* k–ε models have been carried out with the standard "Yap" correction term and also with a new differential form of such term "NYP" which is free from any explicit wall distance.

3.2.1. Zonal k–ε model

In this turbulence model the Reynolds stresses and heat fluxes are obtained via the eddy-viscosity and eddy-diffusivity approximations respectively:

$$\overline{u_i u_j} = -\nu_t\left(\frac{\partial U_i}{\partial x_j} + \frac{\partial U_j}{\partial x_i}\right) + 2/3\delta_{ij}k \tag{5}$$

$$\overline{u_i \theta} = -\frac{\nu_t}{\sigma_\theta}\frac{\partial \Theta}{\partial x_i} \tag{6}$$

and the turbulent viscosity, ν_t, is obtained from

$$\nu_t = c_\mu \frac{k^2}{\varepsilon} \tag{7}$$

To obtain ν_t, the computational domain is divided into two regions: the fully turbulent region and the low-Reynolds-number near-wall region. Within the fully turbulent region the standard high-*Re* k–ε model is used. In this turbulence model the transport equations for k and ε are written as

$$\frac{\partial}{\partial x_j}(U_j k) = \frac{\partial}{\partial x_j}\left[\left(\frac{\nu_t}{\sigma_k}\right)\frac{\partial k}{\partial x_j}\right] + P_k - \varepsilon \tag{8}$$

$$\frac{\partial}{\partial x_j}(U_j \varepsilon) = \frac{\partial}{\partial x_j}\left[\left(\frac{\nu_t}{\sigma_\varepsilon}\right)\frac{\partial \varepsilon}{\partial x_j}\right] + c_{\varepsilon 1}\frac{\varepsilon}{k}P_k - c_{\varepsilon 2}\frac{\varepsilon^2}{k} \tag{9}$$

where P_k, the generation rate of turbulent kinetic energy, is obtained from Eq. (10)

$$P_k = -\overline{u_i u_j}\frac{\partial U_i}{\partial x_j} \tag{10}$$

The coefficients in Eqs. (6)–(9) are given in Table 1.

For modeling of the near-wall region, a simple low-*Re* one-equation model is employed. The equation for the

Table 1
Empirical constants for the k–ε model

c_μ	$c_{\varepsilon 1}$	$c_{\varepsilon 2}$	σ_k	σ_ε	σ_θ
0.09	1.44	1.92	1.0	1.3	0.9

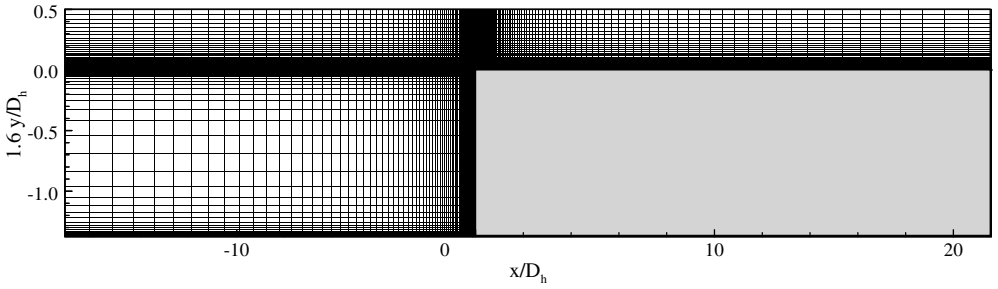

Fig. 4. Computational grid with 181×110 nodes in stream-wise (x) and cross-stream (y) directions.

Table 2
Values of coefficients in the non-linear k–ε model

c_1	c_2	c_3	c_4	c_5	c_6	c_7
−0.1	0.1	0.26	$-10c_\mu^2$	0	$-5c_\mu^2$	$5c_\mu^2$

turbulent kinetic energy is the same as that in the standard k–ε model (Eq. (8)). The dissipation rate, ε, is calculated from a prescribed near-wall length-scale according to the algebraic expression

$$\varepsilon = k^{3/2}/\ell_\varepsilon \tag{11}$$

where the length-scale ℓ_ε is expressed by

$$\ell_\varepsilon = 2.55y[1 - \exp(-0.236y^*)] \tag{12}$$

y is the normal distance to the wall and y^* is a turbulent Reynolds number defined as

$$y^* = yk^{1/2}/v \tag{13}$$

The turbulent viscosity is now obtained from

$$v_t = c_\mu \ell_\mu k^{1/2} \tag{14}$$

where

$$\ell_\mu = 2.55y[1 - \exp(-0.016y^*)] \tag{15}$$

and c_μ is the same as that in the standard k–ε eddy-viscosity model.

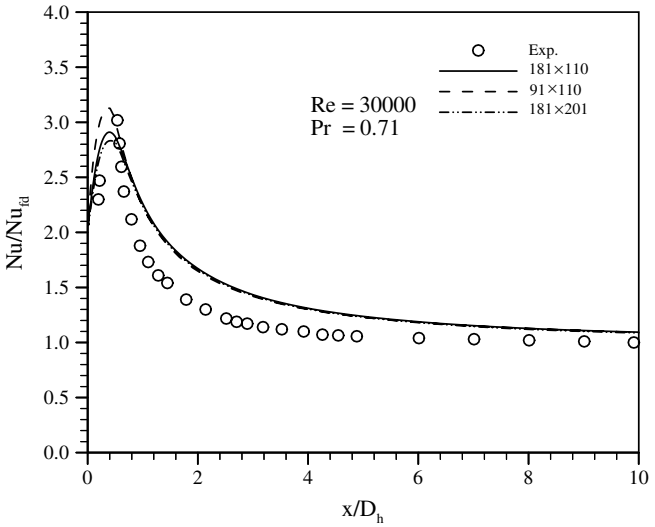

Fig. 5. Predicted local Nusselt number using the linear k–ε model with the "Yap" term using fine (91×110) finer (181×110) and finest (181×201) grids.

3.2.2. Linear low-Re k–ε model

In this turbulence model the Reynolds stresses and heat fluxes are also obtained using Eqs. (5) and (6) while the turbulent viscosity, v_t, is obtained from

$$v_t = c_\mu f_\mu \frac{k^2}{\tilde{\varepsilon}} \tag{16}$$

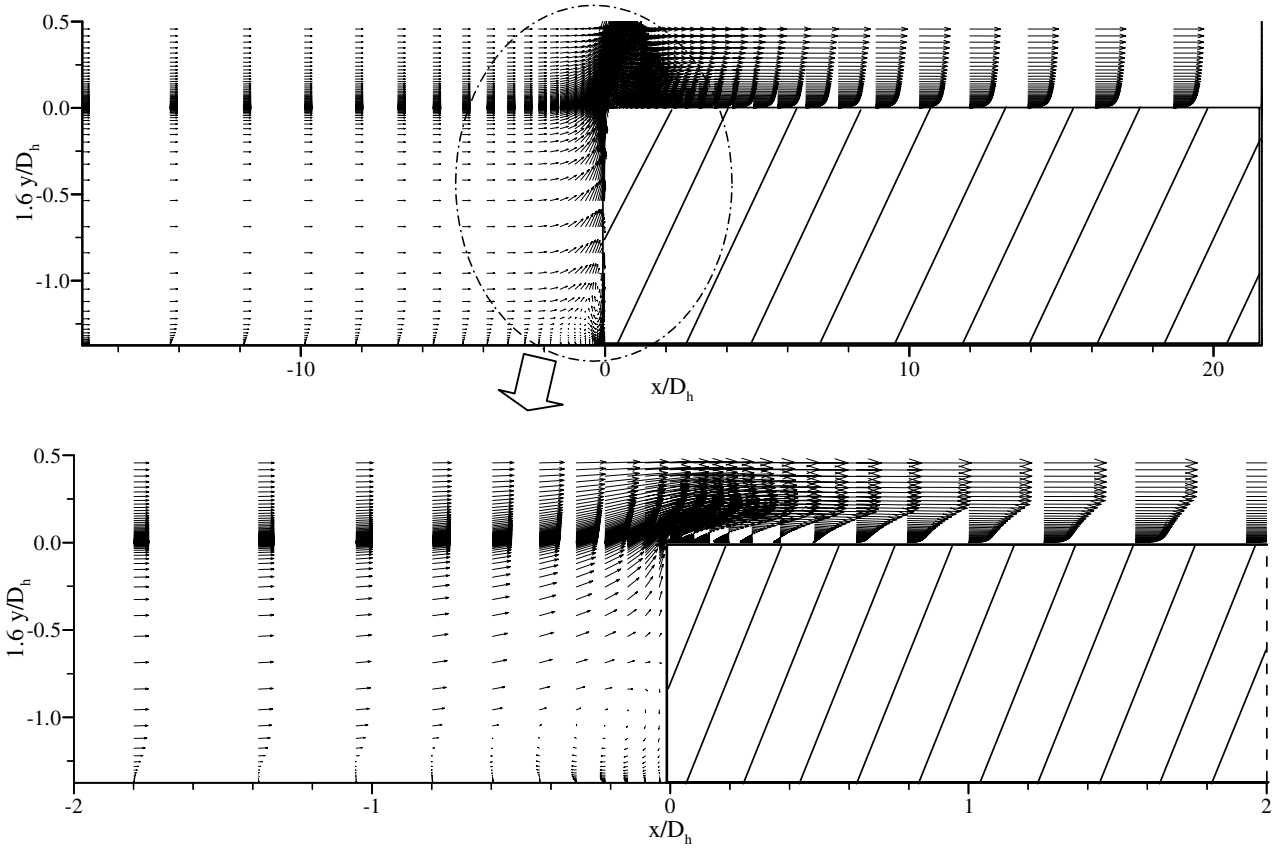

Fig. 6. Predicted mean flow field for $Re = 3.0 \times 10^4$ using the linear k–ε model with the "NYP" term.

To obtain v_t, transport equations for the turbulence kinetic energy, k, and homogeneous dissipation rate, $\tilde{\varepsilon}$, are solved. The transport equation for turbulent kinetic energy is written as

$$\frac{\partial}{\partial x_j}(U_j k) = \frac{\partial}{\partial x_j}\left[\left(v + \frac{v_t}{\sigma_k}\right)\frac{\partial k}{\partial x_j}\right] + P_k - \tilde{\varepsilon} - 2v\left(\frac{\partial \sqrt{k}}{\partial x_j}\right)^2 \tag{17}$$

The dissipation rate of turbulent kinetic energy is obtained by solving the equation

$$\frac{\partial}{\partial x_j}(U_j \tilde{\varepsilon}) = \frac{\partial}{\partial x_j}\left[\left(v + \frac{v_t}{\sigma_\varepsilon}\right)\frac{\partial \tilde{\varepsilon}}{\partial x_j}\right] + c_{\varepsilon 1}\frac{\tilde{\varepsilon}}{k}P_k - c_{\varepsilon 2} f_2 \frac{\tilde{\varepsilon}^2}{k} + E + S_\varepsilon \tag{18}$$

As mentioned above, the variable $\tilde{\varepsilon}$ is the homogeneous dissipation rate which can be related to the true dissipation rate through

$$\tilde{\varepsilon} = \varepsilon - 2v\left(\frac{\partial \sqrt{k}}{\partial x_j}\right)^2 \tag{19}$$

The damping functions f_μ and f_2 are given by

$$f_\mu = \exp[-3.4/(1 + 0.02\widetilde{R}_t)^2]$$
$$f_2 = 1 - 0.3\exp(-\widetilde{R}_t^2) \tag{20}$$

where $\widetilde{R}_t = k^2/v\tilde{\varepsilon}$ is the local turbulent Reynolds number.

The model constants are the same as those given in Table 1. The term E was first introduced by Jones and Launder (1972) and is expressed as

$$E = 2v v_t\left(\frac{\partial^2 U_i}{\partial x_j \partial x_k}\right)^2 \tag{21}$$

The extra source term, S_ε, stands for the "Yap" or "NYP" correction terms which are discussed in the end of this section.

3.2.3. Non-linear low-Re k–ε model

In this turbulence model, turbulent stresses are obtained via the constitutive relation

$$\begin{aligned}\overline{u_i u_j} = {} & 2/3k\delta_{ij} - v_t S_{ij} + c_1\frac{v_t k}{\tilde{\varepsilon}}(S_{ik}S_{kj} - 1/3S_{kl}S_{kl}\delta_{ij}) \\ & + c_2\frac{v_t k}{\tilde{\varepsilon}}(\Omega_{ik}S_{kj} + \Omega_{jk}S_{ki}) \\ & + c_3\frac{v_t k}{\tilde{\varepsilon}}(\Omega_{ik}\Omega_{jk} - 1/3\Omega_{lk}\Omega_{lk}\delta_{ij}) \\ & + c_4\frac{v_t k^2}{\tilde{\varepsilon}^2}(S_{ki}\Omega_{lj} + S_{kj}\Omega_{li})S_{kl} \\ & + c_5\frac{v_t k^2}{\tilde{\varepsilon}^2}(\Omega_{il}\Omega_{lm}S_{mj} + S_{il}\Omega_{lm}\Omega_{mj} - 2/3S_{lm}\Omega_{mn}\Omega_{nl}\delta_{ij}) \\ & + c_6\frac{v_t k^2}{\tilde{\varepsilon}^2}S_{ij}S_{kl}S_{kl} + c_7\frac{v_t k^2}{\tilde{\varepsilon}^2}S_{ij}\Omega_{kl}\Omega_{kl},\end{aligned} \tag{22}$$

where S_{ij} and Ω_{ij} are strain and vorticity rate tensors

$$S_{ij} = \left(\frac{\partial U_i}{\partial x_j} + \frac{\partial U_j}{\partial x_i}\right) \quad \Omega_{ij} = \left(\frac{\partial U_i}{\partial x_j} - \frac{\partial U_j}{\partial x_i}\right) \tag{23}$$

The turbulent heat fluxes, $\overline{u_i\theta}$, are modeled using the simple eddy-diffusivity approximation as in Eq. (6). The model coefficients, c_1 to c_7, have been calibrated by Craft et al. (1993), by reference to several flows, including homogeneous shear flows, swirling flows and curved channel flows. The values of these coefficients are given in Table 2.

The k and $\tilde{\varepsilon}$ transport equations and eddy-viscosity formulation are similar to those of linear model, however, for modeling of c_μ the following expression was proposed by Craft et al. (1999):

$$c_\mu = \min\left[0.09, \frac{12}{1 + 3.5\eta + f_{RS}}\right] \tag{24}$$

with

$$\eta = \max(\widetilde{S}, \widetilde{\Omega}) \tag{25}$$

where the strain and vorticity invariants are expressed as

$$\widetilde{S} = \frac{k}{\tilde{\varepsilon}}\sqrt{0.5S_{ij}S_{ij}}, \quad \widetilde{\Omega} = \frac{k}{\tilde{\varepsilon}}\sqrt{0.5\Omega_{ij}\Omega_{ij}} \tag{26}$$

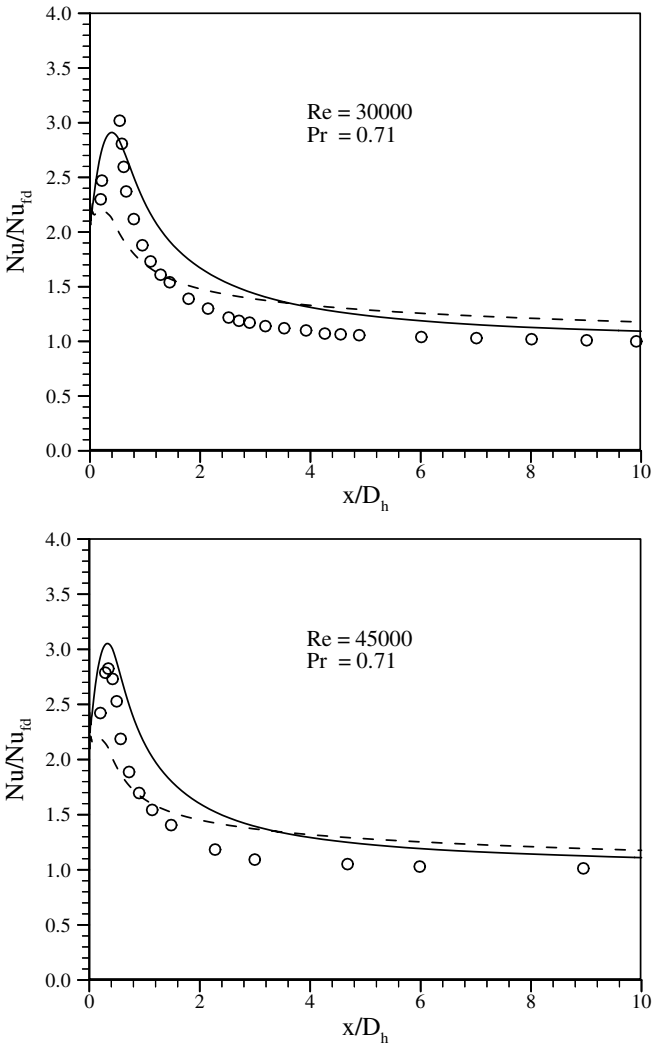

Fig. 7. Predicted local Nusselt number: ○ exp., - - - zonal k–ε model, — linear k–ε model with the "Yap" term.

and

$$f_{RS} = 0.235[\max(0, \eta - 3.333)]^2 \exp(-\widetilde{R}_t/400) \tag{27}$$

The viscous damping function of ν_t is provided by the function f_μ

$$f_\mu = 1 - \exp\left\{-\left(\frac{\widetilde{R}_t}{90}\right)^{1/2} - \left(\frac{\widetilde{R}_t}{400}\right)^2\right\} \tag{28}$$

The near-wall source term E is now expressed as

$$E = \begin{cases} 0.0022\frac{\widetilde{S}\nu_t k^2}{\tilde{\varepsilon}}\left(\frac{\partial^2 U_i}{\partial x_j \partial x_k}\right)^2 & \widetilde{R}_t \leqslant 250 \\ 0 & \widetilde{R}_t > 250 \end{cases} \tag{29}$$

3.2.4. Length-scale correction terms

It is well-known that, in separated flows, the Launder and Sharma version of ε-equation returns excessively high levels of near-wall turbulence. To address this problem, Yap (1987) introduced an extra source term into the dissipation rate equation, "Yap", based on the wall distance, y:

$$S_\varepsilon = \text{Yap} = 0.83\frac{\tilde{\varepsilon}^2}{k}\max[(\ell/\ell_e - 1)(\ell/\ell_e)^2, 0] \tag{30}$$

where ℓ is the turbulent length-scale $k^{3/2}/\tilde{\varepsilon}$, the equilibrium length-scale $\ell_e = 2.55y$, and y is the distance to the wall.

To eliminate the dependence of the above source term on the wall distance, a differential form of the length-scale correction proposed by Iacovides and Raisee (1999)

$$\text{NYP} = \max\left[C_\omega F(F+1)^2\frac{\tilde{\varepsilon}^2}{k}, 0\right] \tag{31}$$

where

$$F = \{[(\partial\ell/\partial x_j)(\partial\ell/\partial x_j)]^{1/2} - \mathrm{d}\ell_e/\mathrm{d}y\}/C_\ell, \tag{32}$$

represents the difference between the predicted length-scale gradient, with $\ell = k^{3/2}/\tilde{\varepsilon}$, and the "equilibrium length-scale gradient", $\mathrm{d}\ell_e/\mathrm{d}y$, defined by

$$\mathrm{d}\ell_e/\mathrm{d}y = C_\ell[1 - \exp(-B_\varepsilon\widetilde{R}_t)] + B_\varepsilon C_\ell\widetilde{R}_t\exp(-B_\varepsilon\widetilde{R}_t) \tag{33}$$

where $C_\ell = 2.55$, $B_\varepsilon = 0.1069$ and

$$C_\omega = \frac{0.83\min(1, \widetilde{R}_t/5)}{[0.8 + 0.7(\eta'/3.33)^4\exp(-\widetilde{R}_t/12.5)]}$$
$$\eta' = \max\left[\frac{k}{\tilde{\varepsilon}}, \sqrt{\nu/\varepsilon}\right]\eta \tag{34}$$

The limited $\widetilde{R}_t$ dependent damping is included for numerical stability.

4. Numerical solver

In the present study the transport equations are solved using finite-volume methodology in a semi-staggered grid

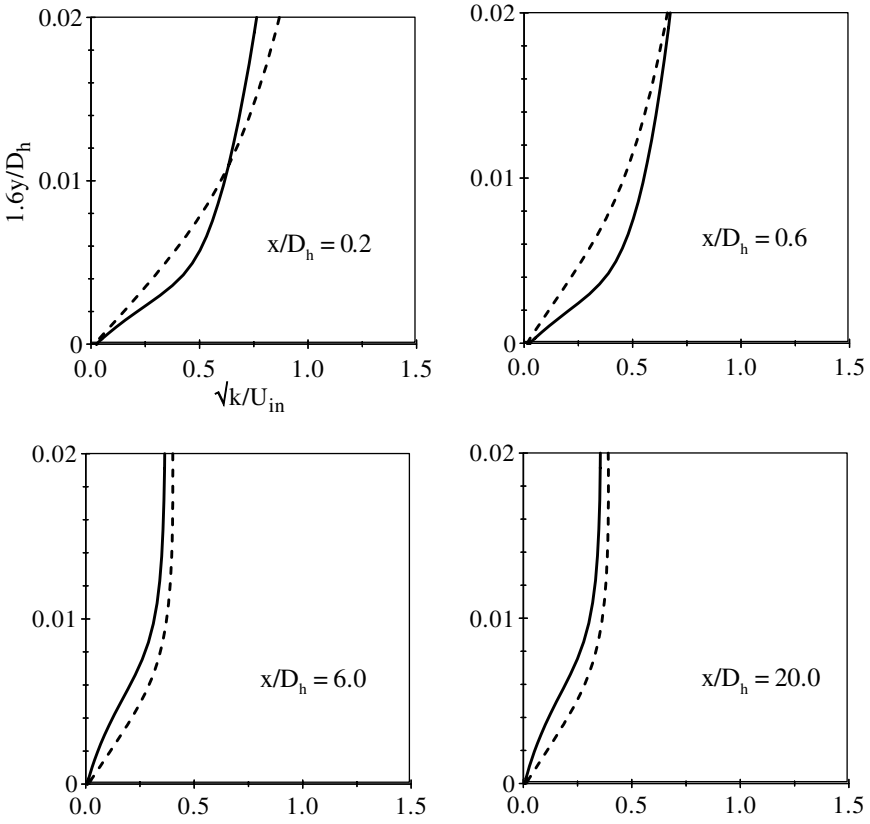

Fig. 8. Predicted near-wall turbulent kinetic energy: - - - zonal k–ε model, — linear k–ε model with the "Yap" term, $Re = 3.0\times10^4$, $Pr = 0.71$.

system. In such a grid distribution, both velocity components are computed and stored in the same nodal position and the velocity nodes are located at the corners of the scalar control volume. The hybrid differencing scheme is employed for approximation of the convective terms in all transport equations. The pressure field is linked to that of velocity through the well-known SIMPLE pressure correction algorithm. To avoid stability problems associated with pressure–velocity decoupling the Rhie and Chow (1983) interpolation scheme is also employed.

Due to the symmetry of the channel, computations were performed only for half of the channel. The grid used for preliminarily computations consists of (91×110) grid nodes in the stream-wise (x) and cross-stream (y) directions respectively. Although, the grid in the cross-stream direction is quite fine, the computational mesh in the stream-wise direction is felt to need further refinement to resolve the velocity and temperature gradients in the recirculation region accurately. Thus, the grid nodes in the stream-wise direction are doubled and, as shown in Fig. 4, a finer computational mesh which consists of (181×110) grids is employed.

For the first test case ($Re = 3.0 \times 10^4$), the influence of this grid refinement on heat transfer predictions of the linear k–ε model is shown in Fig. 5. It is seen that the differences between the predicted local Nusselt number on the fine (91×110) and finer (181×110) meshes are fairly small indicating that the numerical results are reasonably grid-independent. In order to investigate the (181×110) mesh is sufficient to yield grid-independent solutions; a further grid refinement has been undertaken by adding 91 nodes in y-direction. It is noted that the predicted local Nusselt number on this finest (181×201) mesh showed no major changes in heat transfer predictions. Thus, results obtained on the (181×110) mesh are regarded as grid-independent.

All the results presented here have been obtained using 181×110 mesh. In the stream-wise direction, half of the nodes (90) are located upstream of the contraction and the rest (91 nodes) are positioned downstream of the channel contraction. In the cross-stream direction 45 nodes cover the height of the contraction while the rest (65 nodes) are placed across the narrow part of the channel. In all computations, the y^+ values of the near-wall nodes were kept less than unity. In the zonal k–ε model, the first 15 grid nodes are within the fixed-length-scale region and at the interface between the near-wall and the fully turbulent regions the y^* value is around 100.

Flow and heat transfer through the channels examined in this investigation are governed by elliptic partial differential equations, and these require the prescription of boundary conditions along the entire perimeter of the solution domain. Along the symmetry axis, the normal velocity component is set to zero and the values of all other variables at the boundary are set to those at the nearest cell inside the computational domain. Subsequently, the corresponding coefficients in the discretized equations are set to zero. Due to the use of low-Reynolds-number turbulence models to resolve the near-wall region, no special treatment is necessary for the wall boundary conditions of the mean flow and turbulence transport equations. The velocity components, turbulent kinetic energy, and homogeneous dissipation rate are set to zero along the solid walls. As mentioned earlier, the walls of channel downstream of the contraction are under a uniform heat flux boundary condition. To implement this condition, in the discretized temperature equation, the link coefficient is set to zero. Subsequently, an extra source term is included in the discretized temperature equation for the near-wall temperature control volumes of the form

$$S_\Theta = \frac{q''_w}{c_p} A_{cell} \tag{35}$$

where A_{cell} is the wall area of the control volume and c_p is the specific heat capacity of the fluid.

The wall temperature is then determined from the values of the near-wall temperature and heat flux according to

$$\Theta_w = \Theta_I + \frac{q''_w Pr \Delta y}{\mu c_p} \tag{36}$$

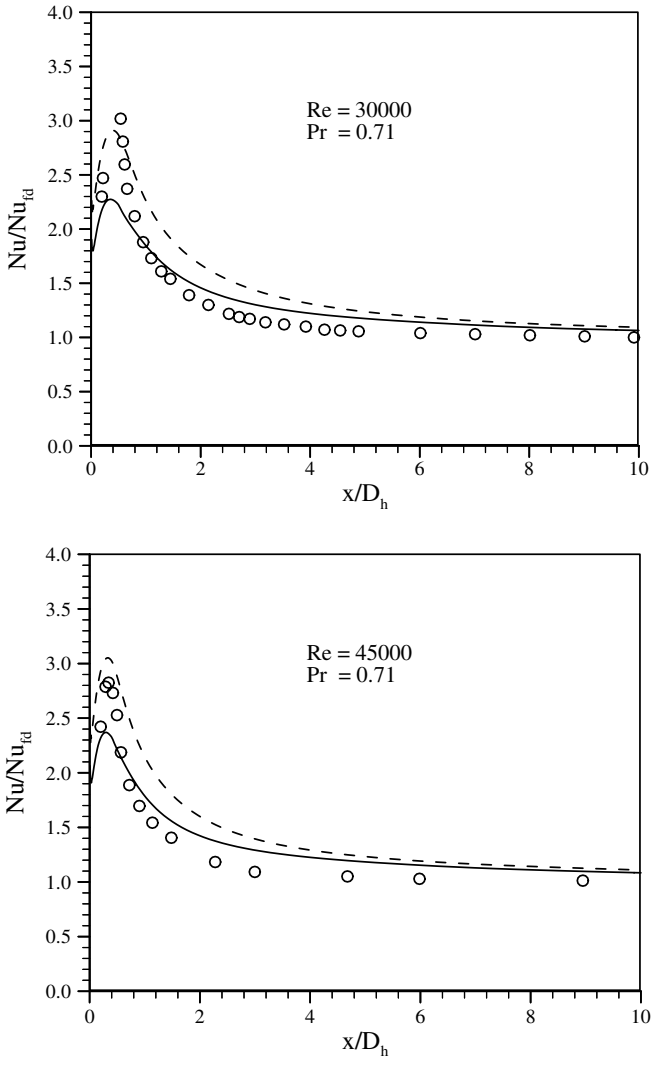

Fig. 9. Predicted Nusselt number: ○ exp., - - - linear k–ε model with the "Yap" term, — linear k–ε model with the "NYP" term.

where Θ_I is the temperature at the node nearest to the wall, and Δy stands for the distance from the wall. For adiabatic walls, the wall temperatures are set equal to the temperature of the adjacent control volumes inside the computational domain and in the discretized temperature equation the link coefficient to the wall is set to zero. At the inlet of computational domain, uniform flow and temperature fields are imposed. A zero stream-wise gradient condition is applied across the outlet boundary for all variables except pressure and temperature. For the pressure, a uniform bulk correction is applied on pressure at the exit plane in order to satisfy the mass continuity. For the thermal field outlet condition, the second derivation of temperature is set equal to zero.

5. Results and discussion

Fig. 6 shows the predicted velocity vectors using the linear k–ε model with the "Yap" term at $Re = 3.0 \times 10^4$. An enlargement of the contraction region is also included, to highlight the more interesting features of the flow development. The velocity vectors returned by the non-linear k–ε model and the zonal k–ε model were similar and thus are not shown here. The vector plot indicates that the flow uniformly enters the channel and develops along the wider section of the channel. Part of flow then impinges on the vertical wall of contraction and is divided into two parts, one part flows downward and creates a large vortex in the corner of channel while the second part moves upward and enters the narrower part of channel.

As shown with the enlarged velocity vectors in Fig. 6, the flow separates immediately at the channel contraction and reattaches on the wall at a position about half one hydraulic diameter downstream of the channel contraction. As a result of this process, a small but intense recirculation bubble is created at the narrower channel inlet. Downstream of the reattachment point, the flow builds up a new boundary layer as it develops along the channel. The predicted sizes of recirculation bubble at $Re = 3.0 \times 10^4$ are $0.575D_h$, $0.57D_h$ and $0.48D_h$ using the linear, the non-linear and the zonal k–ε models respectively which are in reasonable agreement with the experimental value of $0.5D_h$ reported by Han and Park (1988). Moreover, the predicted sizes of recirculation bubble at $Re = 4.5 \times 10^4$ are $0.452D_h$, $0.45D_h$ and $0.42D_h$ using the linear, the non-linear and the zonal k–ε models which are in acceptable agreement with the value of $0.4D_h$ measured by Sparrow and Cur (1982).

In Fig. 7 the distribution of the local Nusselt numbers ratio (Nu/Nu_{fd}) returned by the zonal k–ε model and the linear k–ε model with the "Yap" term are compared with the measured data. At both Reynolds numbers, measurements indicate that the Nusselt number reaches its peak value at a position close to the flow reattachment point

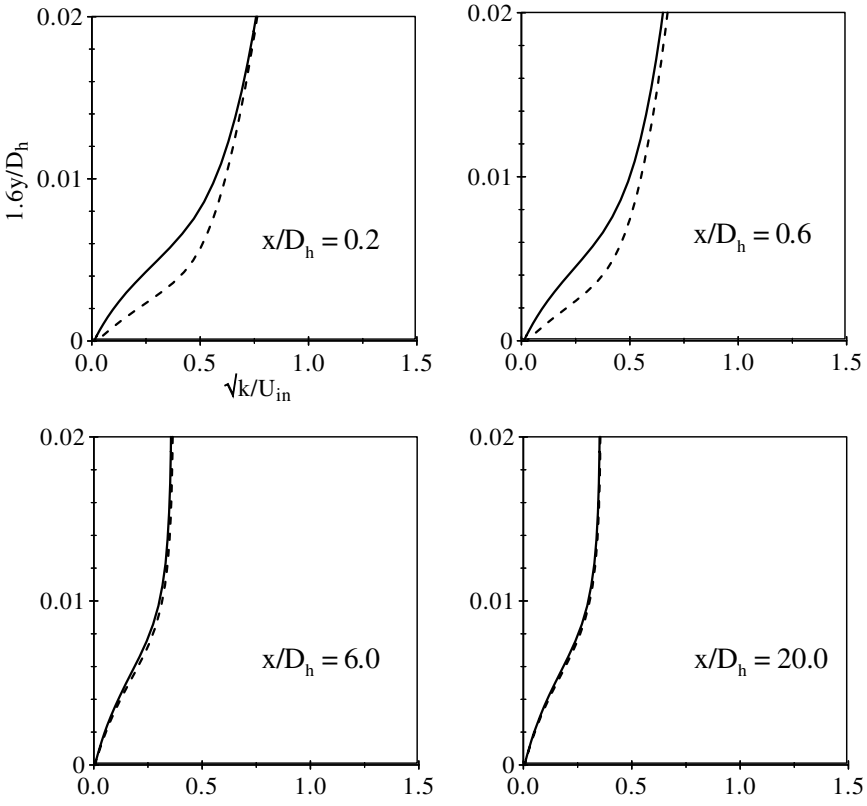

Fig. 10. Predicted near-wall turbulent kinetic energy: - - - linear k–ε model with the "Yap" term, — linear k–ε model with the "NYP" term, $Re = 3.0 \times 10^4$, $Pr = 0.71$.

then drops and eventually reaches to its fully developed value.

As can be noted from Fig. 6, the reasons for the high heat transfer levels immediately after the contraction are the flow separation, the mixing of flow in the recirculation bubble and the flow reattachment. At both Reynolds numbers, it is seen that the zonal k–ε model fails to predict the measured distribution of local Nusselt number. In the separation region downstream of the contraction, the zonal k–ε model underpredicts the measured data whilst in developing region overpredicts them. For both test cases, the predicted distribution of the local Nusselt number using the linear k–ε model is similar to the experimental data although the measured data are somewhat overpredicted in developing region.

These predictive differences are consistent with the near-wall turbulent kinetic energy levels returned by the zonal and linear low-*Re* k–ε models shown in Fig. 8. As can be seen within the separation bubble, e.g. $x/D_h = 0.2$, the near-wall turbulent kinetic energy levels of the zonal k–ε model are lower than those of the linear k–ε model, whilst outside the separation bubble, e.g. $x/D_h = 20$, the linear k–ε model returns higher near-wall turbulent kinetic energy. This feature indicates that the heat transfer predictions of low-*Re* turbulence models depend on the near-wall turbulence energy returned by these models.

The predicted Nusselt number ratios using the linear k–ε model with the "Yap" and "NYP" correction terms are shown in Fig. 9. For both Reynolds numbers, although the replacement of the "Yap" correction term with the "NYP" term underpredicts the peak Nusselt number, it somewhat improves the heat transfer predictions in the developing region downstream of the flow reattachment point, i.e. $0.5 < x/D_h < 6$. Note that far from the contraction, i.e. $x/D_h > 6$, the low-*Re* k–ε model with either length-scale correction terms return similar Nusselt number values. To explain these predictive differences, the near-wall distributions of turbulence energy returned by the low-*Re* k–ε models are shown in Fig. 10. As can be noted, within the separation bubble and close to the reattachment point, the "NYP" term returns somewhat lower turbulence levels than the "Yap" term. Whilst further downstream, e.g. $x/D_h > 6$, the near-wall turbulent kinetic energy levels of both length-scale correction terms are more or less the same, a feature consistent with the heat transfer comparisons.

In Fig. 11 the thermal performances of the linear and non-linear k–ε models in predicting the distribution of local Nusselt number are compared. Both sets of computation were performed with the inclusion of the "NYP" length-scale correction term in the dissipation rate equation.

As also noted in Fig. 9, the linear k–ε model with the "NYP" term somewhat underpredicts the Nusselt numbers within the separation region and slightly overpredicts them outside the separation region. It is clearly seen that the implementation of the non-linear model goes some way to remove these predictive weaknesses of the linear model and returns somewhat better Nusselt number predictions both within the recirculation bubble and also in developing region outside the separation bubble. However, for both test cases the peak Nusselt number is still underpredicted, and at the higher Reynolds number a rather different behavior is seen at $x/D_h = 0$. As can be observed from comparisons shown in Fig. 12, these predictive differences of the linear and non-linear low-*Re* k–ε models are consistent with the near-wall turbulence energy returned by theses models. These comparisons indicate that the heat transfer performance of low-*Re* turbulence models (at least in part) depends on their ability in reproducing the near-wall turbulence.

6. Conclusions

This paper discusses comparisons between heat transfer predictions and measurements for developing flow through

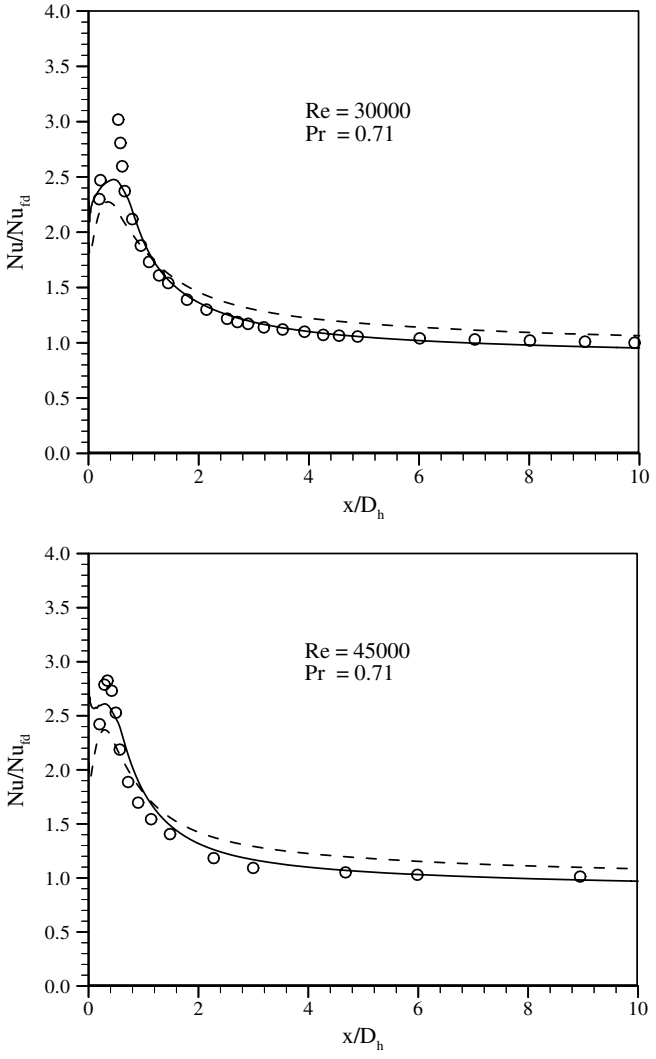

Fig. 11. Predicted Nusselt number: ○ exp., - - - linear k–ε model with the "NYP" term, — non-linear k–ε model with the "NYP" term.

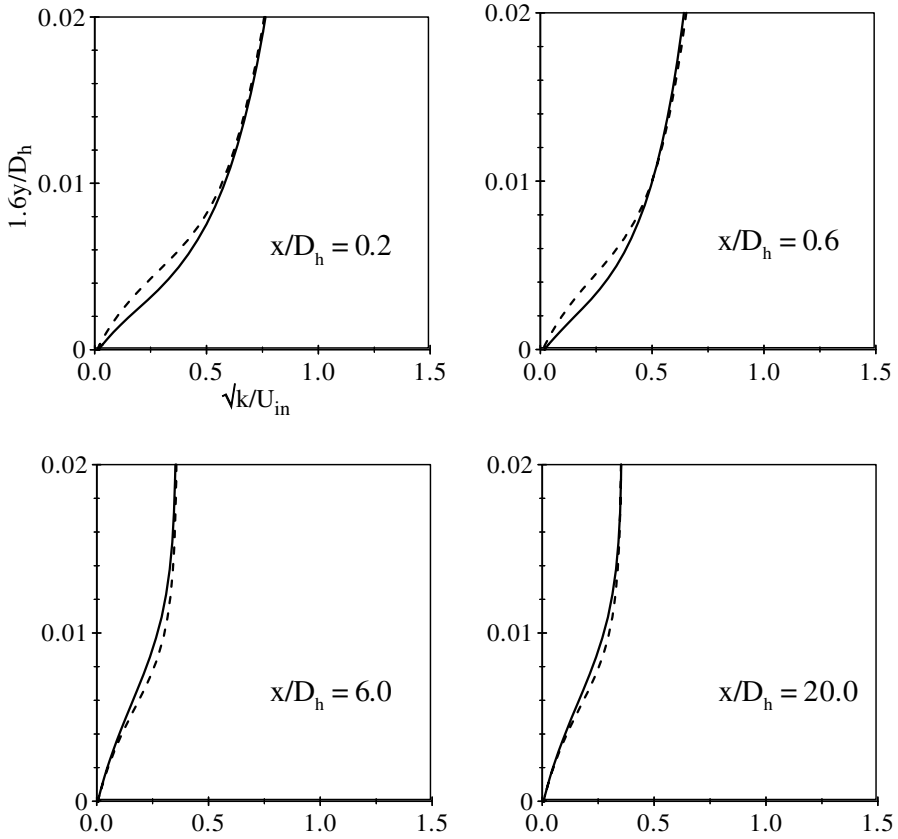

Fig. 12. Predicted near-wall turbulent kinetic energy: - - - linear k–ε model with the "NYP" term, — non-linear k–ε model with the "NYP" term, $Re = 3.0 \times 10^4$, $Pr = 0.71$.

straight channels with a sudden contraction at a junction. The investigation shows that a small recirculation bubble is created immediately downstream of the contraction which subsequently influences the variation of local heat transfer coefficient and increases the heat transfer levels by a factor of three. Computational results show that the zonal k–ε model produces an incorrect Nusselt number distribution by underpredicting the heat transfer levels in the recirculation bubble and overpredicting them in the developing region. It is shown that this is caused by the near-wall turbulence energy returned by this model. The linear low-*Re* k–ε model with the "Yap" term returns correct Nusselt distribution along the channel wall, though it somewhat overpredicts the heat transfer levels in the developing region. The replacement of the "Yap" term with the "NYP" term in linear low-*Re* k–ε model reduces the near-wall turbulent kinetic energy levels and as a result produces too low heat transfer levels within the separation region; although it predicts better local Nusselt number levels outside the recirculation region. The application of the non-linear k–ε model slightly improves the thermal predictions. In general, among the three turbulence models examined, the non-linear low-*Re* k–ε model with the "NYP" length-scale correction term produces the best heat transfer predictions. From the predictions presented in this paper, it can be concluded that the thermal performance of the low-*Re* turbulence models depends on their ability to reproduce the turbulence energy in the near-wall region.

References

Bo, T., Iacovides, H., Launder, B.E., 1991. The prediction of convective heat transfer in rotating square ducts, 8th Symp. on Turbulent Shear Flows, Munich, Germany, pp. 24.4.1–24.4.6.

Craft, T.J., Launder, B.E., Suga, K., 1993. Extending the applicability of eddy viscosity models through the use of deformation invariants and non-linear elements. In: Proc. 5th Int. Symp. Refined Flow Modeling and Turbulence Measurements, Paris, pp. 125–132.

Craft, T.J., Iacovides, H., Yoon, J.H., 1999. Progress in the use of non-linear two-equation models in the computation of convective heat transfer in impinging and separated flows. Turbulence Flow Combust. 63, 59–80.

Han, J.C., Park, J.S., 1988. Developing heat transfer in rectan-gular channels with rib turbulators. Int. J. Heat Mass Transfer 31, 183–195.

Iacovides, H., Raisee, M., 1999. Recent progress in the computation of flow and heat transfer in internal cooling passages of gas turbine blades. Int. J. Heat Fluid Flow 20, 320–328.

Jones, W.P., Launder, B.E., 1972. The prediction of laminarization with a two equation model of turbulence. Int. J. Heat Mass Transfer 15, 301–314.

Launder, B.E., Sharma, B.I., 1974. Application of the energy dissipation model of turbulence to the calculation of flow near a spinning disc. Lett. Heat Mass Transfer 1, 131–138.

Liou, T., Hwang, J., 1992. Developing heat transfer and friction in a ribbed rectangular duct with flow separation at inlet. ASME J. Heat Transfer 114, 565–573.

Raisee, M., Noursadeghi, A., Iacovides, H., 2003. Application of a non-linear k–ε model in prediction of convective heat transfer through ribbed passages. Int. J. Numer. Methods Heat Fluid Flow 14 (3), 285–304.

Raisee, M., Alemi, H., Iacovides, H., 2006. Prediction of developing turbulent flow in 90° curved ducts using linear and non-linear low-Re k–ε models. Int. J. Numer. Methods Fluids 51, 1379–1405.

Rhie, C.M., Chow, W.L., 1983. Numerical study of the turbulent flow past an airfoil with trailing edge separation. AIAA J. 21, 1525–1532.

Sparrow, E.M., Cur, N., 1982. Turbulent heat transfer in a symmetrically or asymmetrically heated flat rectangular duct with flow separation at inlet. ASME J. Heat Transfer 104, 82–89.

Yap, C.R., 1987. Turbulent heat and momentum transfer in recirculation and impinging flows. Ph.D. Thesis, Faculty of Technology, University of Manchester.